VLSI Implementation of a Pipelined 128 points 4-Parallel radix-2³ FFT Architecture via Folding Transformation

James J. W. Kunst `jjwk89@gmail.com`
Kevin H. Viglianco `kevinviglianco@gmail.com`
Daniel R. Garcia `dani6rg@gmail.com`

Digital Signal Processing in Very Large Scale Integration Systems

Autumn 2019

Dr. Keshab K. Parhi
Dr. Ariel L. Pola

Universidad Nacional de Córdoba - FCEFyN
Av.Vélez Sársfield 1611, X5016GCA, Córdoba, Argentina

Fundación FULGOR
Ernesto Romagosa 518, Colinas V. Sarsfield, X5016GQN, Córdoba, Argentina

Abstract—- This work describes the design and the VLSI implementation of a 4-parallel pipelined architecture for the complex fast Fourier transform (CFFT) based on the radix-2³ algorithm with 128 points using folding transformation and register minimization techniques. In addition, different synthesis reports from the Hardware Description Language (HDL) using different optimization techniques were studied in order to obtain good performance on speed and area with a clock frequency of $500MHz$ using an open-source FreePDK45 of 45 nm CMOS technology [9].

I. INTRODUCCION

The Fast Fourier Transform (FFT) is widely used in different applications fields, particularly in algorithms that involves applying digital signal processing, e.g., calculate the Discrete Fourier Transform (DFT) efficiently. Nowadays is common to use parallel-pipelined architecture in FFT algorithms for real time applications, this allows to achieve good performance with high throughput rates.

There are two main types of pipelined FFT architectures [1]. On one hand, feedback architectures (FB) which can be divided into Single-path Delay Feedback (SDF) and Multi-path Delay Feedback (MDF), both methods transfer data samples between stages serially and use feedback loops. On the other hand, feedforward architectures such as Multi-Path Delay Commutator (MDC) transfers more than one sample per clock cycle and do not use feedback loops.

This work focuses on the design of 4-parallel pipelined architecture *radix*-2³ 128-points for Complex FFT-DIF (Decimation In Frequency). Section II, describes the equations that correspond to Butterfly structure of *radix*-2³ FFT-DIF. In Section III, the design of a 2-parallel pipelined architecture, *radix*-2³ 16-points FFT via folding transformation is presented. In

Section IV, the previous design is translate to a 4-parallel, 128-points *radix*-2³ DIF complex FFT, and a float-point simulator in *Matlab* is elaborated, to later be compared with a fixed-point model in order to obtain the best Signal to Quantization Noise Ratio (SQNR). In Section **??**, different power, area and timing reports with different optimizations such as varying pipelining levels, and the application of canonical signed digit (CSD) are compared to obtain the best performance with a clock frequency of $500MHz$. Finally in Section VI, some conclusions and discussions are presented.

II. RADIX-2³ FFT ALGORITHM

The N-point DFT of an input sequence $x[n]$ is defined as:

$$X[k] = \sum_{n=0}^{N-1} x[n]\dot{W}_N^{nk}, \quad k = 0, 1, ..., N-1 \quad (1)$$

where $W_N^{nk} = e^{-j\frac{2\pi}{N}nk}$.

Direct computation of the DFT is basically inefficient, primarily because it does not exploit the symmetry and periodicity properties of the phase factor W_N, these two properties are:

$$\text{Symmetry property: } W_N^{k+N/2} = -W_N^k \quad (2)$$

$$\text{Periodicity property: } W_N^{k+N} = W_N^k \quad (3)$$

The FFT design based on Cooley-Tukey algorithm is most commonly used to compute the DFT efficiently, this allows to reduce the number of operations from $O(N^2)$ to $O(Nlog_2N)$. The development of computationally efficient algorithms for DFT is possible if a *Divide and Conquer* approach is adopted. This approach is based on the decomposition of an N point
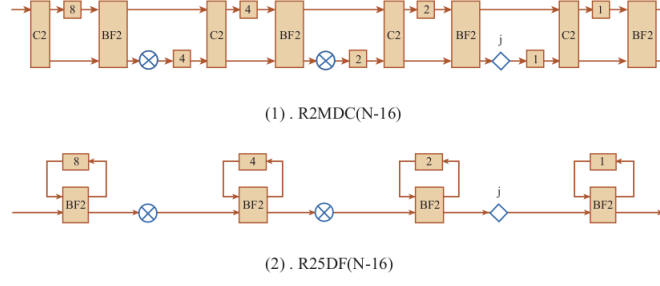
Figure 1: Types of pipelined FFT archicectures for 16 points [**?**].

DFT into successively smaller DFTs, this means that the DFT is calculated as a series of $s = log_\rho N$ stages, where ρ is the base of the *radix*, e.g., in this work this factor is two, so the number of stages for 128 points is 7.

According to [2], [3], There are two methods to design FFT algorithms:

a) Decimation in time (DIT): In this method the N-point data sequence $x[n]$ is split into two $N/2$-point data sequences, thus, is possible to obtain two different functions by decimating $x[n]$ by a factor of 2. The decimation of the data sequence can be repeated again, until the resulting sequences are reduced to one-point sequence.

b) Decimation in frequency (DIF): This method is based on the divide-and-conquer technique, where the DFT formula is split into two summations, one of which involves the sum over the first $N/2$ data points and the second sum involves the last $N/2$ data points.

In each decomposition, the basic computing unit that processes the samples is called *butterfly*. In general, each butterfly involves one complex multiplication and two complex additions. The main difference between DIT and DIF is the instant in which the multiplication by W_N^ϕ is computed, the input samples can be multiplied before or after the butterfly structure, as is depicted in Fig.2.
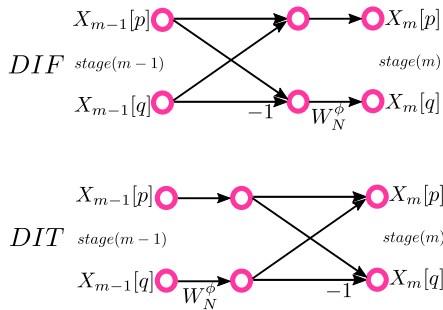

Figure 2: Basic butterflies computation in the decimation in time and frequency.

Another difference between the two methods is that the input samples in DIF algorithms are organized in natural order but the output are not in order, in which case a reordering circuit at the output is needed, in contrast with the DIT algorithms where the input sequence are not in order but the output is in natural order.

According to the methodology presented in [2], it is possible to apply the mathematical expressions of *radix-2^3* DIF as is

explain in [4]. These fundamental equations are describe in equation (4):

$$C_{8k+0} = \sum_{n=0}^{N/8-1} \left\{ [(x_n + x_{n+\frac{N}{2}}) + (x_{n+\frac{N}{4}} + x_{n+\frac{3N}{4}})] + \right. \tag{4}$$

$$\left. [(x_{n+\frac{N}{8}} + x_{n+\frac{5N}{8}}) + (x_{n+\frac{3N}{8}} + x_{n+\frac{7N}{8}})] \right\} W_N^{0n} W_{N/8}^{nk}$$

$$C_{8k+4} = \sum_{n=0}^{N/8-1} \left\{ [(x_n + x_{n+\frac{N}{2}}) + (x_{n+\frac{N}{4}} + x_{n+\frac{3N}{4}})] - \right.$$

$$\left. [(x_{n+\frac{N}{8}} + x_{n+\frac{5N}{8}}) + (x_{n+\frac{3N}{8}} + x_{n+\frac{7N}{8}})] \right\} W_N^{4n} W_{N/8}^{nk}$$

$$C_{8k+2} = \sum_{n=0}^{N/8-1} \left\{ [(x_n + x_{n+\frac{N}{2}}) - (x_{n+\frac{N}{4}} + x_{n+\frac{3N}{4}})] - j \right.$$

$$\left. [(x_{n+\frac{N}{8}} + x_{n+\frac{5N}{8}}) - (x_{n+\frac{3N}{8}} + x_{n+\frac{7N}{8}})] \right\} W_N^{2n} W_{N/8}^{nk}$$

$$C_{8k+6} = \sum_{n=0}^{N/8-1} \left\{ [(x_n + x_{n+\frac{N}{2}}) - (x_{n+\frac{N}{4}} + x_{n+\frac{3N}{4}})] + j \right.$$

$$\left. [(x_{n+\frac{N}{8}} + x_{n+\frac{5N}{8}}) - (x_{n+\frac{3N}{8}} + x_{n+\frac{7N}{8}})] \right\} W_N^{6n} W_{N/8}^{nk}$$

$$C_{8k+1} = \sum_{n=0}^{N/8-1} \left\{ [(x_n - x_{n+\frac{N}{2}}) - j(x_{n+\frac{N}{4}} - x_{n+\frac{3N}{4}})] + W_N^{N/8} \right.$$

$$\left. [(x_{n+\frac{N}{8}} - x_{n+\frac{5N}{8}}) - j(x_{n+\frac{3N}{8}} - x_{n+\frac{7N}{8}})] \right\} W_N^{n} W_{N/8}^{nk}$$

$$C_{8k+5} = \sum_{n=0}^{N/8-1} \left\{ [(x_n - x_{n+\frac{N}{2}}) - j(x_{n+\frac{N}{4}} - x_{n+\frac{3N}{4}})] - W_N^{N/8} \right.$$

$$\left. [(x_{n+\frac{N}{8}} - x_{n+\frac{5N}{8}}) - j(x_{n+\frac{3N}{8}} - x_{n+\frac{7N}{8}})] \right\} W_N^{5n} W_{N/8}^{nk}$$

$$C_{8k+3} = \sum_{n=0}^{N/8-1} \left\{ [(x_n - x_{n+\frac{N}{2}}) + j(x_{n+\frac{N}{4}} - x_{n+\frac{3N}{4}})] + W_N^{3N/8} \right.$$

$$\left. [(x_{n+\frac{N}{8}} - x_{n+\frac{5N}{8}}) + j(x_{n+\frac{3N}{8}} - x_{n+\frac{7N}{8}})] \right\} W_N^{3n} W_{N/8}^{nk}$$

$$C_{8k+7} = \sum_{n=0}^{N/8-1} \left\{ [(x_n - x_{n+\frac{N}{2}}) + j(x_{n+\frac{N}{4}} + x_{n+\frac{3N}{4}})] - W_N^{3N/8} \right.$$

$$\left. [(x_{n+\frac{N}{8}} - x_{n+\frac{5N}{8}}) + j(x_{n+\frac{3N}{8}} - x_{n+\frac{7N}{8}})] \right\} W_N^{7n} W_{N/8}^{nk}$$

Fig. 3 and Fig. 4 show the equivalent diagram of interconnections and data flows from the equations presented in (4).
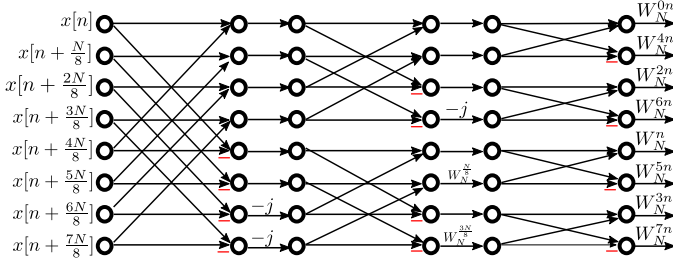
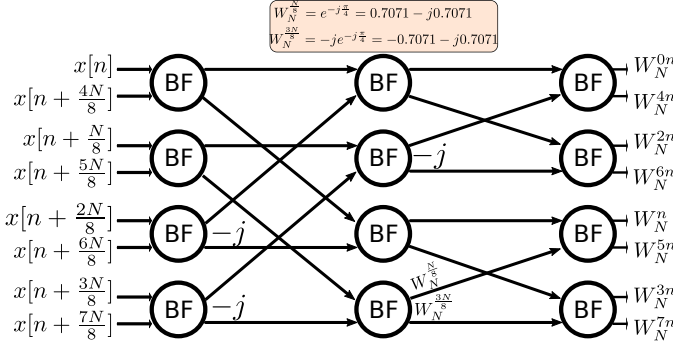Figure 3: Structure of interconnection for *radix*-2^3 DIF DFT.

Figure 4: Data flow graph (DFG) based in equations (4).

A. 16 points DFT

The next step is to find the suitable rotator factors for the 16 point DFT, the equations in (4) are essential for this design and they were evaluated to get $C_{8k+i} = \sum_{n=0}^{16/8-1}\{\cdot\}$, for $k = 0, 1$. The structure for the 16 point DFT is described in Fig. 5 and Fig. 6.
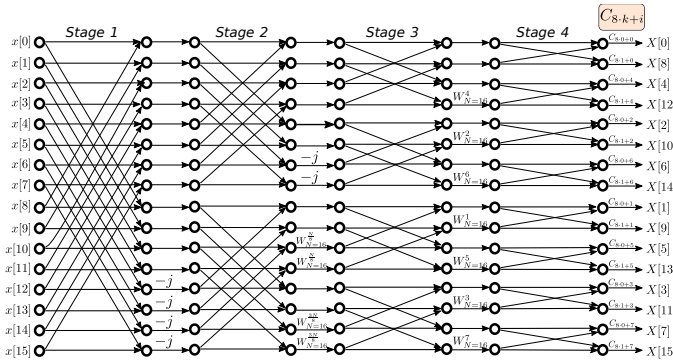

Figure 5: Flow graph of a *radix*-2^3 16-point DIF DFT

B. 128 points DFT

With these first approaches is possible the application of the divide and conquer strategy by decomposing the 128-point DFT and calculating each coefficient $C_{8k+i} = \sum_{n=0}^{128/8-1}\{\cdot\}$, for $k = 0, 1, ..., (128/8) - 1$, this way a chain sequence of butterflies is obtained together with its corresponding rotation factor and the correct index of the samples in which they must be added or multiplied. Using this technique is possible to do a subdivision of butterflies stages, as is shown in Fig. 7, the decomposition of the 128 point DFT involves three stages of butterflies resulting in a set of eight 16 point DFTs. Finally,
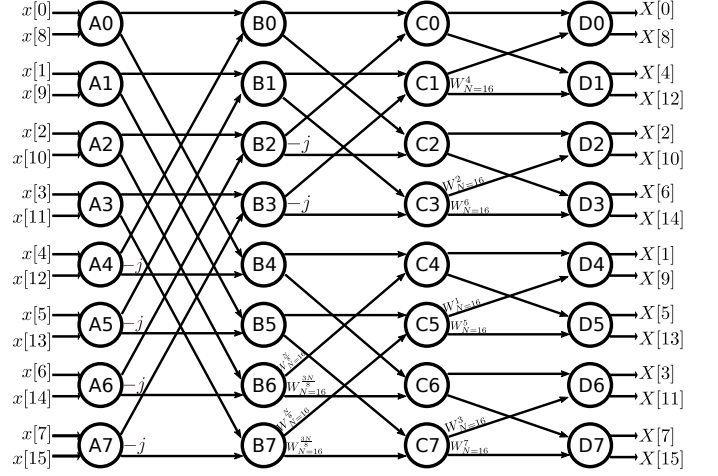

Figure 6: Data flow graph (DFG) for a *radix*-2^3 16-point DIF DFT

Fig. 8 shows the complete architecture for the *radix*-2^3 128-point DIF DFT with a total of seven stages where each stage contains 64 butterflies of radix-2 base.

III. Design of a FFT architecture via folding transformation

In this section, the architecture proposed in [5] together with the folding transformation and register minimization techique described in [6] is used to obtain a 16-point DIF FFT 4-parallel architecture, then, the same method is extended to achieve a 128-point DIF FFT 4-parallel architecture.

A. 4-Parallel radix-2^3 16-Points

The flow graph of a 16-point DIF FFT radix-2^3 with main base radix-2 is shown in Fig. 5. The graph is divided into four stages, each of them consist of a set of butterflies and multipliers. The twiddle factor between the stages indicates a multiplication by W_N^k, where W_N denotes the Nth root of unity, with its exponent evaluated modulo N. This can be represented as a DFG as shown in Fig. 6, where the nodes represents the butterfly computations of the radix-2 FFT algorithm.

The folding transformation is used on the DFG to derive a pipelined architecture, to do this a folding set is needed. A folding set is an ordered set of operations executed by the same functional unit, each folding set contains K entries, where K is called the folding factor. The operation in the jth position within the folding set (where goes from 0 to $K - 1$) is executed by the functional unit during the time partition, this term is called the folding order. In order to derive the folding equations a node graph is needed, where an edge e is consider to connect the nodes U and V with $w(e)$ delays. Let the executions of the lth iteration of the nodes U and V be scheduled at the time units $Kl + u$ and $Kl + v$ respectively, where u and v are the folding orders of the nodes U and V, respectively. The folding equation for the edge e is:

$$D_F(U \to V) = Kw(e) - P_U + v - u \qquad (5)$$

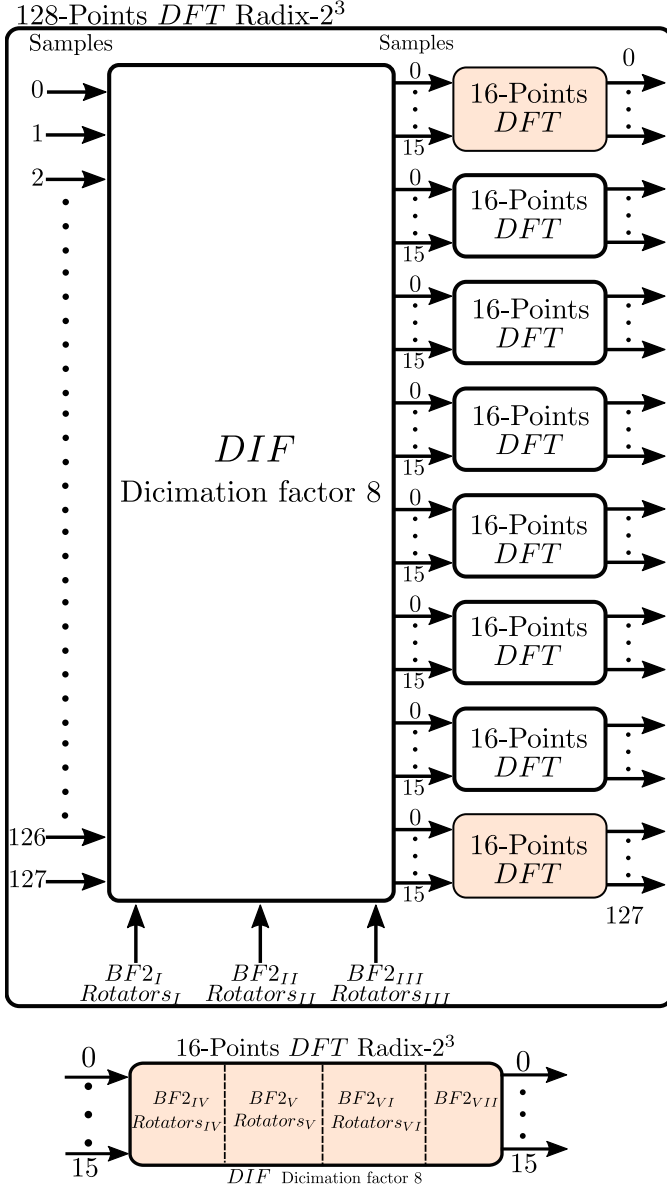where P_U is the number of pipeline stages in the hardware unit which executes the node U.

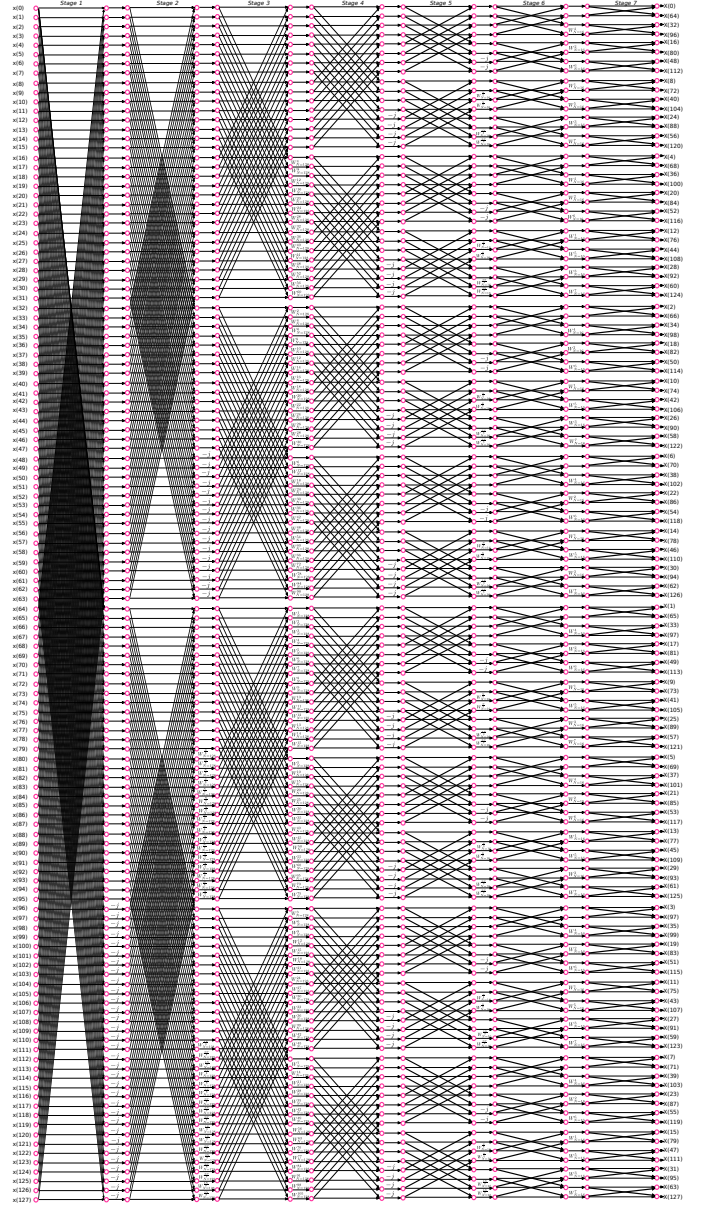## 128-Points DFT Radix-2^3

Figure 7: Decomposing a *radix*-2^3 128-point DFT.

Figure 8: Flow graph of a *radix*-2^3 128-point DIF DFT

Considering the folding of the DFG in Fig. 6 with the folding sets:

$$A = \{A0, A2, A4, A6\} \qquad A' = \{A1, A3, A5, A7\}$$
$$B = \{B1, B3, B0, B2\} \qquad B' = \{B5, B7, B4, B6\}$$
$$C = \{C2, C1, C3, C0\} \qquad C' = \{C6, C5, C7, C4\}$$
$$D = \{D3, D0, D2, D1\} \qquad D' = \{D7, D4, D6, D5\}$$

Assuming that the butterfly operations do not have any pipeline stages ($P_A = P_B = P_C = P_D = 0$), the folding equations can be derived for all edges, thus, the expression *without retiming* can be obtained from (5).

$$D_F(D0 \rightarrow B0) = 2 \qquad D_F(D0 \rightarrow B4) = 2$$
$$D_F(D1 \rightarrow B1) = 0 \qquad D_F(D1 \rightarrow B5) = 0$$
$$D_F(D2 \rightarrow B2) = 2 \qquad D_F(D2 \rightarrow B6) = 2$$
$$D_F(D3 \rightarrow B3) = -1 \qquad D_F(D3 \rightarrow B7) = -1$$
$$D_F(D4 \rightarrow B0) = 0 \qquad D_F(D4 \rightarrow B4) = 0$$
$$D_F(D5 \rightarrow B1) = -1 \qquad D_F(D5 \rightarrow B5) = -1$$
$$D_F(D6 \rightarrow B2) = 0 \qquad D_F(D6 \rightarrow B6) = 0$$
$$D_F(D7 \rightarrow B3) = -2 \qquad D_F(D7 \rightarrow B7) = -2$$
$$D_F(E0 \rightarrow C0) = 1 \qquad D_F(E0 \rightarrow C2) = -2$$
$$D_F(E1 \rightarrow C1) = 1 \qquad D_F(E1 \rightarrow C3) = 2$$
$$D_F(E2 \rightarrow C0) = 0 \qquad D_F(E2 \rightarrow C2) = -3$$
$$D_F(E3 \rightarrow C1) = 0 \qquad D_F(E3 \rightarrow C3) = 1$$
$$D_F(E4 \rightarrow C4) = 1 \qquad D_F(E4 \rightarrow C6) = -2$$
$$D_F(E5 \rightarrow C5) = 1 \qquad D_F(E5 \rightarrow C7) = 2$$
$$D_F(E6 \rightarrow C4) = 0 \qquad D_F(E6 \rightarrow C6) = -3$$
$$D_F(E7 \rightarrow C5) = 0 \qquad D_F(E7 \rightarrow C7) = 1$$
$$D_F(F0 \rightarrow D0) = -2 \qquad D_F(F0 \rightarrow D1) = 0$$
$$D_F(F1 \rightarrow D0) = 0 \qquad D_F(F1 \rightarrow D1) = 2$$

Figure 9: Data Flow graph (DFG) of a radix-2 16-point DIF FFT with retiming and pipeline.

Figure 10: Linear lifetime chart for the variables $y_{(0)}, y_{(1)}, ..., y_{(15)}$ for a 16-point FFT architecture.

Figure 11: Linear lifetime chart for the variables $z_{(0)}, z_{(1)}, ..., z_{(15)}$ for a 16-point FFT architecture.

Figure 12: Linear lifetime chart for the variables $w_{(0)}, w_{(1)}, ..., w_{(15)}$ for a 16-point FFT architecture.

For the folded system to be realizable, $D_F(U \rightarrow V) \geq 0$ must hold for all the edges in the DFG. Retiming and/or pipeline can be applied to satisfy this property, if the DFG in Fig. 6 is pipelined/retimmed as shown in Fig. 9 the system is realizable and the folded delays for the edges are given by the equations that represent a folding set *with retiming*.

$$
\begin{aligned}
D_F(D0 \rightarrow B0) &= 2 & D_F(D0 \rightarrow B4) &= 2 & (6)\\
D_F(D1 \rightarrow B1) &= 4 & D_F(D1 \rightarrow B5) &= 4 \\
D_F(D2 \rightarrow B2) &= 2 & D_F(D2 \rightarrow B6) &= 2 \\
D_F(D3 \rightarrow B3) &= 3 & D_F(D3 \rightarrow B7) &= 3 \\
D_F(D4 \rightarrow B0) &= 0 & D_F(D4 \rightarrow B4) &= 0 \\
D_F(D5 \rightarrow B1) &= 3 & D_F(D5 \rightarrow B5) &= 3 \\
D_F(D6 \rightarrow B2) &= 0 & D_F(D6 \rightarrow B6) &= 0 \\
D_F(D7 \rightarrow B3) &= 2 & D_F(D7 \rightarrow B7) &= 2 \\
D_F(E0 \rightarrow C0) &= 1 & D_F(E0 \rightarrow C2) &= 2 \\
D_F(E1 \rightarrow C1) &= 1 & D_F(E1 \rightarrow C3) &= 2 \\
D_F(E2 \rightarrow C0) &= 0 & D_F(E2 \rightarrow C2) &= 1 \\
D_F(E3 \rightarrow C1) &= 0 & D_F(E3 \rightarrow C3) &= 1 \\
D_F(E4 \rightarrow C4) &= 1 & D_F(E4 \rightarrow C6) &= 2 \\
D_F(E5 \rightarrow C5) &= 1 & D_F(E5 \rightarrow C7) &= 2 \\
D_F(E6 \rightarrow C4) &= 0 & D_F(E6 \rightarrow C6) &= 1 \\
D_F(E7 \rightarrow C5) &= 0 & D_F(E7 \rightarrow C7) &= 1 \\
D_F(F0 \rightarrow D0) &= 2 & D_F(F0 \rightarrow D1) &= 4 \\
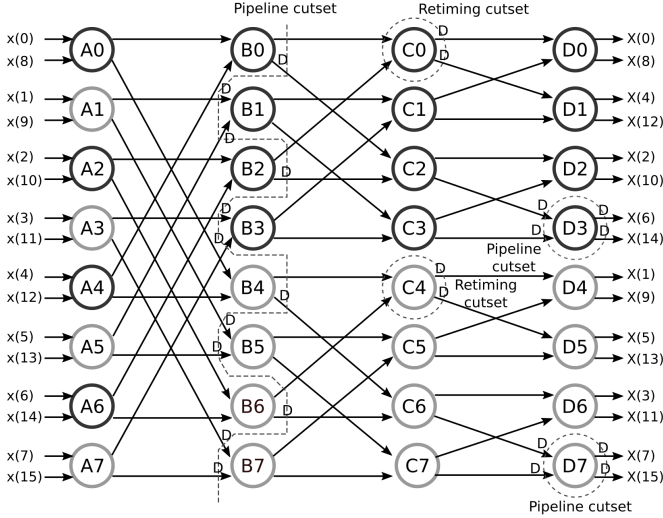D_F(F1 \rightarrow D0) &= 0 & D_F(F1 \rightarrow D1) &= 2 \\
D_F(F2 \rightarrow D2) &= 2 & D_F(F2 \rightarrow D3) &= 4 \\
D_F(F3 \rightarrow D2) &= 0 & D_F(F3 \rightarrow D3) &= 2 \\
D_F(F4 \rightarrow D4) &= 2 & D_F(F4 \rightarrow D5) &= 4 \\
D_F(F5 \rightarrow D4) &= 0 & D_F(F5 \rightarrow D5) &= 2 \\
D_F(F6 \rightarrow D6) &= 2 & D_F(F6 \rightarrow D7) &= 4 \\
D_F(F7 \rightarrow D6) &= 0 & D_F(F7 \rightarrow D7) &= 2
\end{aligned}
$$

The number of registers required to implement the folding equations in (6) is 80, in order to minimize the number of reg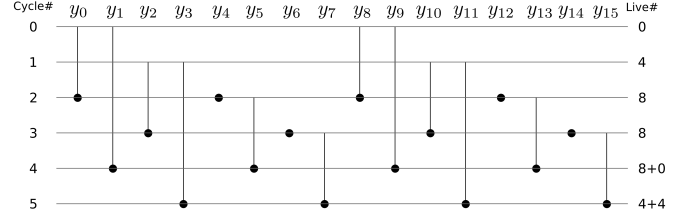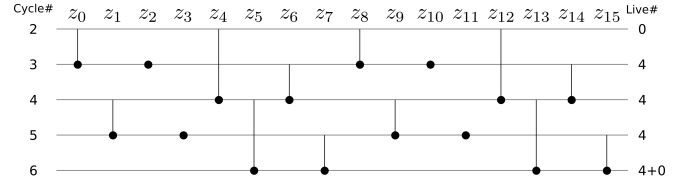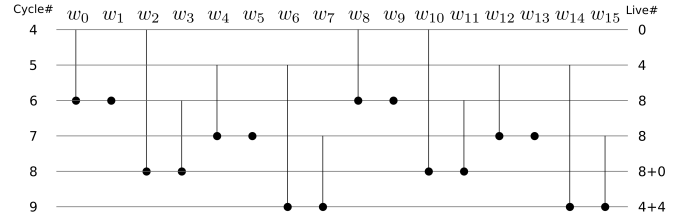isters the register minimization technique is needed. To apply this technique lets consider the output of node $A0$ to be $y_{(0)}$ and $y_{(8)}$, and the output of the node A1 to be $y_{(1)}$ and $y_{(9)}$, applying this method successively with the rest of the nodes A a linear life time chart for this stage is obtain as is shown in Fig.10. Applying this criteria to the rest of the stages the life time chart for nodes B and C are obtained as is shown in Fig.11 and Fig.12 respectively. The resulting maximum number of registers for each stage are 8, 4 and 8 respectively, therefore the total number of registers is reduced from 80 to 20. More information about this method can be found on [6].

The register allocation tables for the lifetime charts are shown in Fig. 13, 14 and 15 for stage A, B and C respectively. Fig.16 and Fig.17 show the designations of registers for the stage A and B respectively used in the allocation tables, the designation for stage C are similar to stage A. The folded architecture in Fig.19 is synthesized using the folding equations and the register allocation tables. The dataflow for each stage can be seen in Tab. I, the control signal for stage A and B can be implemented by dividing the clock signal to 4 and 2 respectively, for stage C the control signal is the same that the stage A. Note that in Fig. 19 the inputs and output are not ordered, to order these variables an extra logic is needed, this imply using more registers and multiplexers.

The inputs for each folding node are represented in a matrix where the values in the same column is the data that flows in

Figure 13: Register allocation table for the data represented in 10

	I/P	R1	R2	R3	R4	R5	R6	R7	R8
0	y0,y8,y1,y9								
1	y2,y10,y3,y11	y1		y0		y9		y8	
2	y4,y12,y5,y13	y3	y1	y2	y0	y11	y9	y10	y8
3	y6,y14,y7,y15	y5	y3	y1	y2	y13	y11	y9	y10
4		y7	y5	y3	y1	y15	y13	y11	y9
5			y7		y3		y15		y11

Figure 14: Register allocation table for the data represented in 11

	I/P	R1	R2	R3	R4
2	z0,z4,z8,z12				
3	z2,z6,z10,z14	z4	z0	z12	z8
4	z1,z5,z9,z13	z6	z4	z14	z12
5	z3,z7,z11,z15	z5	z1	z13	z9
6		z7	z5	z15	z13

parallel, and values in the same row correspond to the data that flows through the same path in consecutive clock cycles. The first two rows represent the inputs of the superior BF and the others two represents the input of the inferior BF. The same criteria is used for represent the rotators constants, where each number k of the matrix represent a multiplication by W_N^k.

The different types of rotators used in Fig. 19 are shown in Fig. 18, the description of each are:

- Trivial rotator: They can be carried out by interchanging the real and imaginary components and/or changing the sign of the data.
- Constant CSD rotator: They can be carried out by interchanging the real and imaginary components and a multiplication by a unique constant fractional number, in this case we will use a CSD multiplier to reduce the area utilized.

	I/P	R1	R2	R3	R4	R5	R6	R7	R8
4	w0,w2,w8,w10								
5	w4,w6,w12,w14	w2		w0		w10		w8	
6	w1,w3,w9,w11	w6	w2	w4	w0	w14	w10	w12	w8
7	w5,w7,w13,w15	w3	w6	w2	w4	w11	w14	w10	w12
8		w7	w3	w6	w2	w15	w11	w14	w10
9			w7		w6		w15		w14

Figure 15: Register allocation table for the data represented in 12
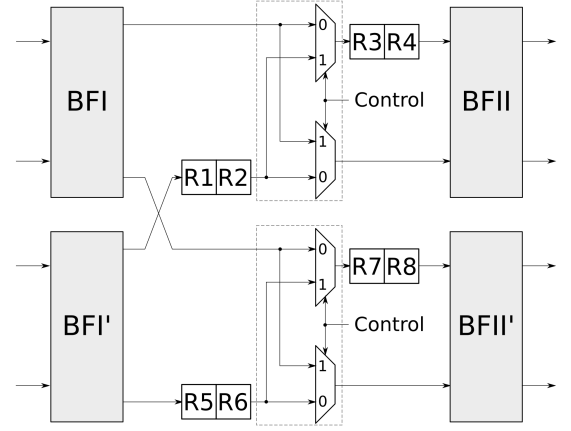
Figure 16: Registers names used in Fig. 13 for stage 1.
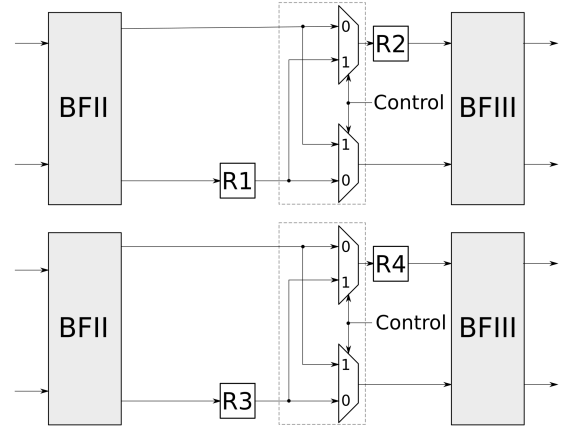
Figure 17: Registers names used in Fig. 14 for stage 2.

- General rotator: They can be carried out by interchanging the real and imaginary components and/or a multiplication by more than one constant fractional numbers, in this case we will use a general multiplier.

IV. 4-PARALLEL RADIX-2^3 128-POINTS

The previously described method can be used in the design of a 4-Parallel radix-2^3 128-Points architecture. The pipelined/retimmed DFG for this design is shown in Fig. 20, the folding sets are listed in Table II, and in Fig.26 the folded architecture is shown.

A. Implementation of a 128-point FFT

In this section the implementation of the 4-parallel architecture for the computation of 128-point *radix*-2^3 DIF complex FFT is described.

Figure 18: Symbols used for the different types of rotators

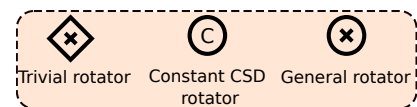| #Cycle	Stage 1		Stage 2		Stage 3	
	Dataflow	Control	Dataflow	Control	Dataflow	Control
0	$y0 \to R3$ $y8 \to R7$	0	$z0 \to R2$ $z8 \to R4$	0	$w0 \to R3$ $w8 \to R7$	0
1	$y2 \to R3$ $y10 \to R7$	0	$(z2, z10) \to i/p$ $R1 \to R2, R3 \to R4$	1	$w4 \to R3$ $w12 \to R7$	0
2	$(y4, y12, R4) \to i/p$ $R2 \to R3, R6 \to R7$	1	$z1 \to R2, z9 \to R4$ $R1 \to i/p, R3 \to i/p$	0	$(w1, w9, R4) \to i/p$ $R2 \to R3, R6 \to R7$	1
3	$(y6, y14, R4) \to i/p$ $R2 \to R3, R6 \to R7$	1	$(z3, z11) \to i/p$ $R1 \to R2, R3 \to R4$	1	$(w5, s9, R4) \to i/p$ $R2 \to R3, R6 \to R7$	1
4	$(R2, R4) \to i/p$	0	$R1 \to i/p, R3 \to i/p$	0	$(R2, R4) \to i/p$	0
5	$(R2, R4) \to i/p$	0	$R1 \to R2, R3 \to R4$	1	$(R2, R4) \to i/p$	0

Table I: Dataflow and mux control for each stage based on registers showed in Figure 16 and 17.
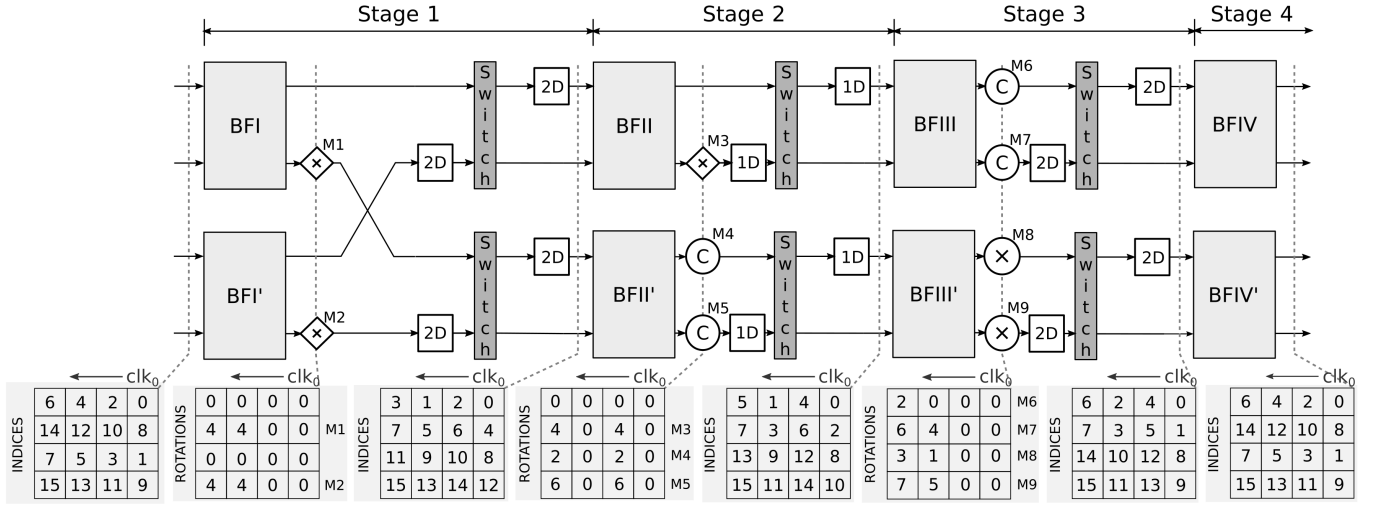

Figure 19: Folding architecture for the computation of a radix-2^3 16-point DIF complex FFT.

Table II: Folding set for the DFG showed in Fig. 20

A	A0 A32	A2 A34	A4 A36	A6 A38	A8 A40	A10 A42	A12 A44	A14 A46	A16 A48	A18 A50	A20 A52	A22 A54	A24 A56	A26 A58	A28 A60	A30 A62
A'	A1 A33	A3 A35	A5 A37	A7 A39	A9 A41	A11 A43	A13 A45	A15 A47	A17 A49	A19 A51	A21 A53	A23 A55	A25 A57	A27 A59	A29 A61	A31 A63
B	B1 B0	B3 B2	B5 B4	B7 B6	B9 B8	B11 B10	B13 B12	B15 B14	B17 B16	B19 B18	B21 B20	B23 B22	B25 B24	B27 B26	B29 B28	B31 B30
B'	B33 B32	B35 B34	B37 B36	B39 B38	B41 B40	B43 B42	B45 B44	B47 B46	B49 B48	B51 B50	B53 B52	B55 B54	B57 B56	B59 B58	B61 B60	B63 B62
C	C16 C17	C18 C19	C20 C21	C22 C23	C24 C25	C26 C27	C28 C29	C30 C31	C1 C0	C3 C2	C5 C4	C7 C6	C9 C8	C11 C10	C13 C12	C15 C14
C'	C48 C49	C50 C51	C52 C53	C54 C55	C56 C57	C58 C59	C60 C61	C62 C63	C33 C32	C35 C34	C37 C36	C39 C38	C41 C40	C43 C42	C45 C44	C47 C46
D	D8 D9	D10 D11	D12 D13	D14 D15	D16 D17	D18 D19	D20 D21	D22 D23	D24 D25	D26 D27	D28 D29	D30 D31	D1 D0	D3 D2	D5 D4	D7 D6
D'	D40 D41	D42 D43	D44 D45	D46 D47	D48 D49	D50 D51	D52 D53	D54 D55	D56 D57	D58 D59	D60 D61	D62 D63	D33 D32	D35 D34	D37 D36	D39 D38
E	E4 E5	E6 E7	E8 E9	E10 E11	E12 E13	E14 E15	E16 E17	E18 E19	E20 E21	E22 E23	E24 E25	E26 E27	E28 E29	E30 E31	E1 E0	E3 E2
E'	E36 E37	E38 E39	E40 E41	E42 E43	E44 E45	E46 E47	E48 E49	E50 E51	E52 E53	E54 E55	E56 E57	E58 E59	E60 E61	E62 E63	E33 E32	E35 E34
F	F2 F3	F4 F5	F6 F7	F8 F9	F10 F11	F12 F13	F14 F15	F16 F17	F18 F19	F20 F21	F22 F23	F24 F25	F26 F27	F28 F29	F30 F31	F1 F0
F'	F34 F35	F36 F37	F38 F39	F40 F41	F42 F43	F44 F45	F46 F47	F48 F49	F50 F51	F52 F53	F54 F55	F56 F57	F58 F59	F60 F61	F62 F63	F33 F32
G	G3 G2	G5 G4	G7 G6	G9 G8	G11 G10	G13 G12	G15 G14	G17 G16	G19 G18	G21 G20	G23 G22	G25 G24	G27 G26	G29 G28	G31 G30	G0 G1
G'	G35 G34	G37 G36	G39 G38	G41 G40	G43 G42	G45 G44	G47 G46	G49 G48	G51 G50	G53 G52	G55 G54	G57 G56	G59 G58	G61 G60	G63 G62	G32 G33

Figure 20: Pipelined/retimmed DFG of a radix-2^3 128-point DIF complex FFT.
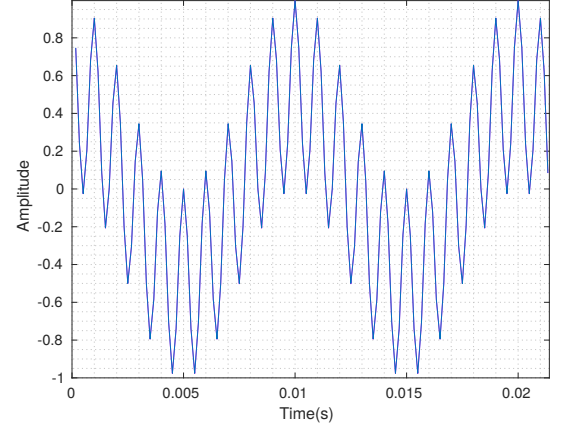

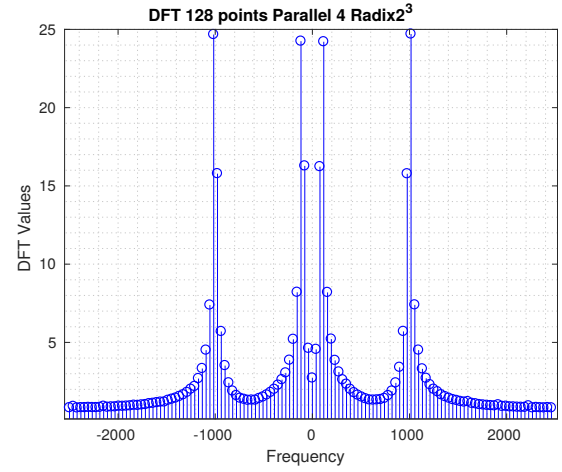Figure 21: Input signal $x[n]$ in time domain

Figure 22: Output samples, absolute value vs frequency $|X[k]|$

In each stage of the Fig. 27, input samples that propagate through the stages will be carefully quantized with the purpose of getting a high SQNR (Signal to Quantization Noise Ratio).

$$SQNR_{dB} =$$
$$10log_{10}\left(\frac{Var\{Signal_{FloatPoint}\}}{Var\{Signal_{FloatPoint} - Signal_{FixedPoint}\}}\right) \quad (9)$$

SQNR computation represents the logarithmic relationship between float signal variance over error variance from an given signal.

The input signal $x[n]$ is quantized with a value of $S(10, 9)$, this representation means a signed (S) number with 10 total bits and 9 fractional bits. The value calculated of SQNR for the input is $56.9dB$. Following the same steps, we can compute the SQNR for the *twiddle* factors and the design output.

Twiddles factor are quantized with a relation of $S(11, 9)$ and the complex output signal $X[k]$ with $S(22, 15)$, output quantization for the real part is $46.8dB$ and for the imaginary part $47.3dB$. In general, a value of quantization close to $50dB$ is a good approximation.

The *MATLAB* fixed-point model is shown in Fig. 27 and Fig.22 shows the output signal in the frequency domain.

In order to compare and validate the operation of the design presented in this work a *MATLAB* simulator has been elaborated to later write a Synthesizable *Verilog* code with different levels of optimizations using a powerful tool like *Synopsys* to get a final design in @45*nm* Standard Cells.

B. Floating and Fixed point Simulator description

The input signal to the design is shown in Fig. 21, the signal will be a mixture of two sinusoid signals with different frequency and normalized amplitude as is describe in equations 7 and 8, where $f_1 = 100Hz$, $f_2 = 1000Hz$ and T_s is the sampled period.

$$x'[n] = cos(2\pi f_1 nT_s) + cos(2\pi f_2 nT_s) \quad (7)$$
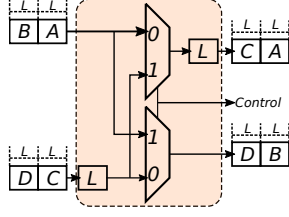$$x[n] = x'[n]/max\{x'[n]\} \quad (8)$$
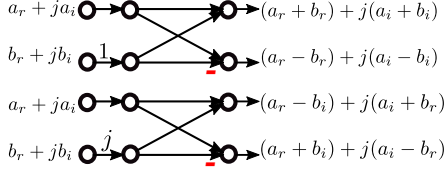
Figure 23: Circuit for data shuffling
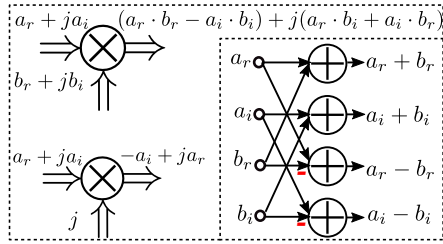

Figure 24: Complex butterfly

Figure 25: Complex multiplier and complex adder

The equivalent circuit of the combination of latencies (delays registers) and switches placed between the stages in Fig. 27 are represented in Fig. 23. This circuits are used to appropriately order samples in each butterflies input.

The combination of latencies (delays registers) and switches placed between the stages in Fig. 27 are used to appropriately order samples in each butterflies input and its equivalent circuit is represented in Fig. 23.

The different elements such as multipliers and butterflies process complex numbers as is shown in Fig. 24 and 25, this means that is essential to divide the signal in its real and imaginary part with the purpose of process them independently.

A *general rotator* (full complex multiplier) computes two multiplications and one addition for the real and imaginary part, as is describe in 25, but in case of a *trivial rotator* (multiplication by i), there are no multiplications of additions, it only swap the numbers and change the sign if is necessary, as is shown in Fig .These relations allows to achieve a good design optimization and are important at the moment of calculating the quantization process to ensure an appropriate quantity of bits.

V. VERILOG (HDL) MODEL ,OPTIMIZATIONS AND RESULTS

In this section the different design instances to model the DFT in hardware will be described. With the purpose to have a global view of the optimization levels to achieve the requested *data arrival time* of $1/500Mhz = 2ns$ and the lowest power consumption, four design have been implemented. The design instances were synthesized by Synopsys tool in order to build an interconnection of Standard Cells and generate a complete set of *timing-area-power report* showed in Table III, IV, V and VI.

The first design was made from the base design showed in Fig.26, this hardware model has butterflies modules that work in combination with multipliers and each multiplier has associated a memory block that contains the twiddle factors. In this first approach all multipliers are *full*, each stage has a control module that enables the inversion of the switching block, this control signal is also sent to the multipliers in order to work synchronously with the switching. To avoid the bit growth generated by the addition and multiplication, a quantization block is necessary, the quantizer consist of saturation and truncate operations. The synthesis report is summarize in Table III, notice that a total power consumption is $695.564mW$ and the data arrival time is greater than minimum period established of $2ns$ resulting in a time violation. In order to minimize the *critical path* and consumption a second design with *pipelined* registers after the quantization blocks was implemented, and also the *trivial* multipliers (multiplication by $-1j$) were implemented in stages one, two and four, this significantly reduced the size of the binary word resulting in a reduction in the total power as is shown in Table IV, however the time violation was still detected in this design. In the third case of optimization an internal pipelined to each butterfly block was added in order to reduce the critical path even more, as the results shown in Table V, this design achieves the data required time. Finally, in the fourth level of optimization showed in Fig.27, the full multipliers from stage two and five were modified to work with *CSD*, achieving a total power consumption of $646.924mW$.

Table III: Design instance 1. Timing-Area-Power Report at 500MHz

Point	Path(ns)
data arrival time	5.60
clock CLK (rise edge)	2.00
clock network delay (ideal)	2.00
library setup time	1.95
data required time	1.95
data arrival time	-5.60
slack (VIOLATED)	-3.65

Logical Elements	
Number of ports	1228
Number of nets	112376
Number of cells	102726
Number of combinational cells	95310
Number of sequential cells	7404
Number of macros/black boxes	0
Number of buf/inv	27817
Combinational area	291201.116637
Buf/Inv area	44892.767764
Noncombinational area	58830.508095
Total cell area	350031.624731

Power Group	Internal	Switching	Leakage	Total Power
io pad	0.0000	0.0000	0.0000	0.0000
clock network	34.8220	603.2268	1.4573e+06	639.6328
register	54.2228	0.2699	4.0540e+05	54.8980
sequential	0.0000	0.0000	0.0000	0.0000
combinational	0.2884	0.7304	1.5016e+04	1.0337
Total	89.333mW	604.227mW	1.877e+06nW	695.564mW

Table IV: Design instance 3. Timing-Area-Power Report at 500MHz

Point	Path(ns)
data arrival time	2.76
clock CLK (rise edge)	2.00
clock network delay (ideal)	2.00
library setup time	1.95
data required time	1.95
data arrival time	-2.76
slack (VIOLATED)	-0.81

Logical Elements	
Number of ports	1571
Number of nets	94523
Number of cells	87311
Number of combinational cells	80220
Number of sequential cells	7076
Number of macros/black boxes	0
Number of buf/inv	23823
Combinational area	233949.801414
Buf/Inv area	36323.350042
Noncombinational area	56229.647552
Total cell area	290179.448967

Power Group	Internal	Switching	Leakage	Total Power
io pad	0.0000	0.0000	0.0000	0.0000
clock network	24.2875	583.5885	1.0269e+06	608.9492
register	51.0349	0.1728	3.8748e+05	51.5952
sequential	0.0000	0.0000	0.0000	0.0000
combinational	0.9554	1.1271	1.8640e+05	2.2689
Total	76.277mW	584.888mW	1.600e+06nW	662.813mW

Table V: Design instance 4. Timing-Area-Power Report at 500MHz

Point	Path(ns)
data arrival time	1.94
clock CLK (rise edge)	2.00
clock network delay (ideal)	2.00
library setup time	1.94
data required time	1.94
data arrival time	-1.94
slack (MET)	0.00

Logical Elements	
Number of ports	2315
Number of nets	75713
Number of cells	66284
Number of combinational cells	58017
Number of sequential cells	8240
Number of macros/black boxes	0
Number of buf/inv	14789
Combinational area	195877.841872
Buf/Inv area	24429.880240
Noncombinational area	64463.046570
Total cell area	260340.888442

Power Group	Internal	Switching	Leakage	Total Power
io pad	0.0000	0.0000	0.0000	0.0000
clock network	18.1655	581.6307	7.8320e+05	600.6672
register	58.2275	0.2873	4.4422e+05	58.9591
sequential	0.0000	0.0000	0.0000	0.0000
combinational	0.7768	0.9958	1.5970e+05	1.9322
Total	77.169mW	582.913mW	1.387e+06nW	661.558mW

Table VI: Design instance 5. Timing-Area-Power Report at 500MHz

Point	Path(ns)
data arrival time	1.94
clock CLK (rise edge)	2.00
clock network delay (ideal)	2.00
library setup time	1.94
data required time	1.94
data arrival time	-1.94
slack (MET)	0,00

Logical Elements	
Number of ports	2192
Number of nets	55840
Number of cells	48628
Number of combinational cells	40551
Number of sequential cells	8054
Number of macros/black boxes	0
Number of buf/inv	9158
Combinational area	134844.907554
Buf/Inv area	14112.789311
Noncombinational area	64112.010178
Total cell area	198956.917732

Power Group	Internal	Switching	Leakage	Total Power
io pad	0.0000	0.0000	0.0000	0.0000
clock network	19.9015	560.4803	4.9715e+05	580.8741
register	61.1289	1.4388	4.4180e+05	63.0096
sequential	0.0000	0.0000	0.0000	0.0000
combinational	1.5451	1.3368	1.5871e+05	3.0405
Total	82.575mW	563.255mW	1.097e+06nW	646.924mW

factor. Therefore is necessary to add pipeline cutsets and a careful quantization in order to achieve the required sample period with an acceptable SNR.

Folding technique, results in an architecture that uses a large number of register, to avoid this is necessary to apply a register minimization technique and allocate data to these registers. The number of registers applying this method is reduced significantly, from to . This results in a final design with less area and power consumption.

The number of DFT points is related with the radix-base, we can write as *radix*-8, this representation can be expressed as *radix*-2^3 that means we can decompose in smaller radixes with main base-2, an advantage of using a hight radix is reduced the number of multipliers at expense of increase the routing.

The design implemented a quantizer block which works with saturation and truncated, the round method was not used because we reached a high SQNR. Lastly a series of optimization were necessary to accomplish the required frequency. The DFT implementation without any optimization level got to work at 166MHz, applying pipelines cutsets and quantization blocks, the final architecture is implementable at the required clock frequency (500 MHz) at the cost of incrementing the numbers of sequential cells. Finally, with the CSD multipliers, is possible to reduce the combinational cells significantly.

The Fourier Transform without folding technique processes 128 entry points of samples which are ordered but its output are disordered and it is necessary a reordering circuit. In the other hand a Fourier Transform with folding technique also needs a reordering circuit in the input. This circuit present an additional area and power consumption to be considered in the final design.
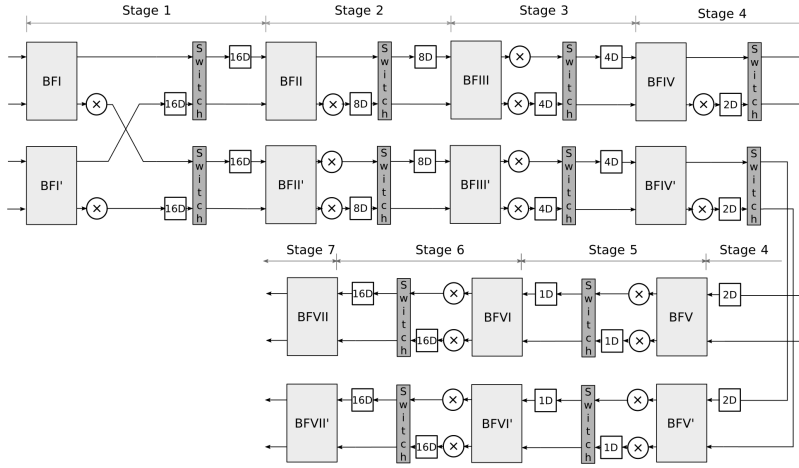
VI. CONCLUSIONS

This work has presented a VLSI Implementation of a Pipelined 128 points 4-Parallel radix-2^3 FFT architecture via folding transformation. The folding transformation applied reduced significantly (equal to the folded factor, i.e. 64 times) the number of functional units, and therefore the silicon area at the expense of increasing the computation time by the same

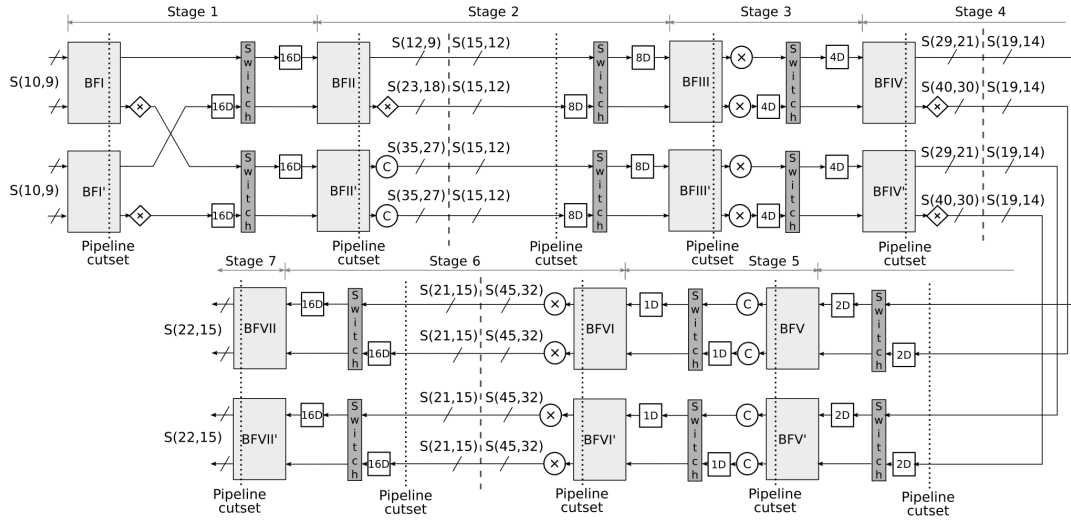Figure 26: Folding architecture for the computation of a radix-2^3 128-point DIF complex FFT.

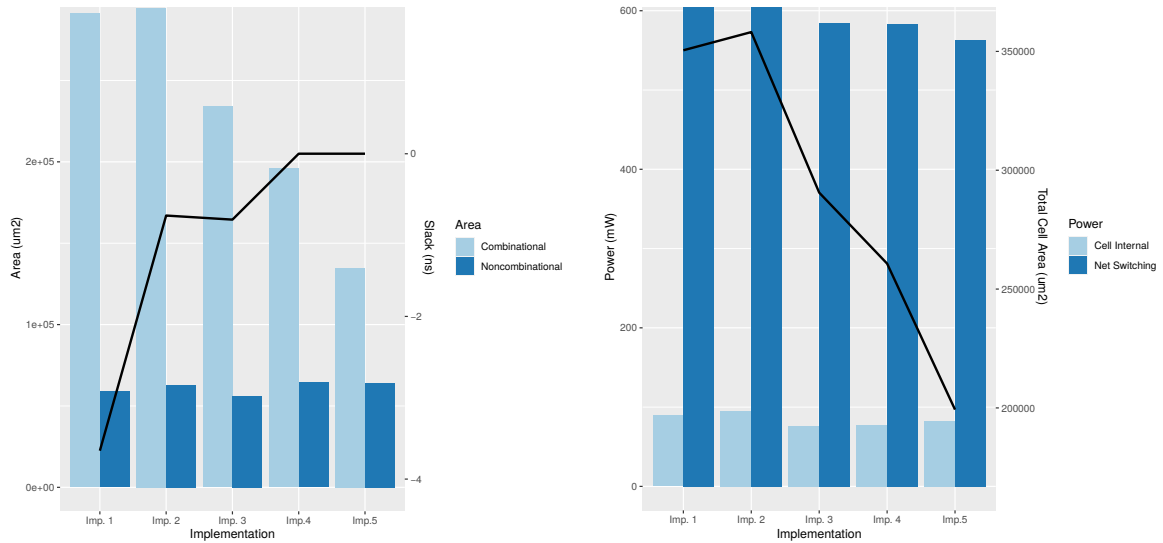Figure 27: Quantization for a 128-point 4-parallel complex FFT architecture

Figure 28: Timing-Area-Power evolution.

REFERENCES

[1] Shousheng He and M. Torkelson, "Designing pipeline FFT processor for OFDM (de)modulation," in *1998 URSI International Symposium on Signals, Systems, and Electronics. Conference Proceedings (Cat. No.98EX167)*. IEEE, pp. 257–262.

[2] J. G. Proakis and D. G. Manolakis, "DIGITAL SIGNAL PROCESSING," p. 1033.

[3] A. V. Oppenheim and R. W. Schafer, *Tratamiento de señales en tiempo discreto, tercera edición*. Pearson Educación, OCLC: 843859190.

[4] L. Jia, Y. Gao, and H. Tenhunen, "Efficient VLSI implementation of radix-8 FFT algorithm," p. 4.

[5] M. Ayinala, M. Brown, and K. K. Parhi, "Pipelined Parallel FFT Architectures via Folding Transformation," *IEEE Transactions on Very Large Scale Integration (VLSI) Systems*, vol. 20, no. 6, pp. 1068–1081, Jun. 2012.

[6] K. K. Parhi, *VLSI Digital Signal Processing Systems. Design and implementation*. JOHN WILEY & SONS, INC., 1999, ch. Folding Transformation, pp. 151–163.

[7] M. Garrido, J. Grajal, M. A. Sanchez, and O. Gustafsson, "Pipelined Radix-2^{k} Feedforward FFT Architectures," *IEEE Transactions on Very Large Scale Integration (VLSI) Systems*, vol. 21, no. 1, pp. 23–32, Jan. 2013.

[8] M. Garrido, S.-J. Huang, and S.-G. Chen, "Feedforward FFT hardware architectures based on rotator allocation," vol. 65, no. 2, pp. 581–592.

[9] R. Thapa, S. Ataei, and J. E. Stine, "WIP. Open-source standard cell characterization process flow on 45 nm (FreePDK45), 0.18 μm, 0.25 μm, 0.35 μm and 0.5 μm," in *2017 IEEE International Conference on Microelectronic Systems Education (MSE)*. Lake Louise, AB, Canada: IEEE, May 2017, pp. 5–6.